Confronting the prediction of leptonic Dirac *CP*-violating phase with experiments

Yang Hwan Ahn,[1,*] Sin Kyu Kang,[1,†] Raymundo Ramos,[1,‡] and Morimitsu Tanimoto[2,§]

[1]*School of Natural Science, Seoul National University of Science and Technology, 232 Gongneung-ro, Nowon-gu, Seoul 01811, Korea*

[2]*Department of Physics, Niigata University, Ikarashi 2-8050, Niigata 950-2181, Japan*

(Received 5 July 2022; accepted 17 October 2022; published 1 November 2022)

We update and improve past efforts to predict the leptonic Dirac *CP*-violating phase with models that predict perturbatively modified tribimaximal or bimaximal mixing. Simple perturbations are applied to both mixing patterns in the form of rotations between two sectors. By translating these perturbed mixing matrices to the standard parametrization for the neutrino mixing matrix we derive relations between the Dirac *CP* phase and the oscillation angles. We use these relations together with current experimental results to constrain the allowed range for the *CP* phase and determine its probability density. Furthermore, we elaborate on the prospects for future experiments probing on the perturbations considered in this work. We present a model with A_4 modular symmetry that is consistent with one of the described perturbed scenarios and successfully predicts current oscillation parameter data.

DOI: 10.1103/PhysRevD.106.095002

I. INTRODUCTION

With the discovery of the Higgs scalar by the LHC in 2012 the standard model (SM) of particle physics took the seat as the most predictive high energy theory so far. While further experimental efforts keep giving results that are mostly consistent with the SM, one of its sectors has, since long ago, given the best motivation for physics beyond the SM: Neutrinos. First proposed as a way to fix conservation laws in beta decays, they have had an eventful history, while they went from massless to having tiny masses and changing flavor—oscillate—while travelling due to mixing between flavor states. The first evidence of neutrino oscillations was reported in 1998 [1]. Neutrino oscillations were firmly established in 2001 using solar neutrinos [2], and, since then, experiments regularly close in on their oscillation pattern and the mass differences responsible for these oscillations. Fast forwarding to 2011 and 2012, the Double Chooz [3] and Daya Bay [4] experiments measured $\theta_{13} \neq 0$ with enough precision to open the possibility of a Dirac type *CP*-violating phase in the mixing of the leptonic sector of the SM described through the Pontecorvo-Maki-Nakagawa-Sakata (PMNS) matrix [5,6].

The usual approach to extend the SM to include neutrino masses and mixing employs a discrete flavor symmetry at a very high energy. After the spontaneous breaking of this symmetry at lower energies, residual symmetries remain in the charged and neutral leptons mass masses, thus, resulting in particular mixing patterns in the PMNS matrix, U^{PMNS}. Before the measurement of the reactor angle, $\theta_{13} \neq 0$, models that predicted no mixing between the first and third family were popular, in particular models that predicted two maximal oscillations popularly known as bimaximal (BM) mixing [7–13] and, as more data accumulated, other works appeared suggesting maximal mixing of two and three families, known as tribimaximal (TBM) mixing [14–17]. Naturally, after the measurement of a nonzero reactor angle, the exact BM and TBM mixing patterns were ruled out. In more complicated formulations, these patterns can be considered the result of residual symmetries that need to be broken by perturbations that permit the appearance of a nonzero reactor angle. Interestingly, these types of formulations often result in relationships between oscillation parameters that allow an estimation of the size of the Dirac type leptonic *CP*-violating phase. This is the idea that was developed in Ref. [18] as well as in several other works [19–40]. In the present work we attempt to follow up on the scenarios explored in Ref. [18] and extend the analysis to probability densities for the *CP*-violating phase based on currently allowed ranges for oscillation parameters from experiments. Moreover, we simulate the effects of the constraints from these scenarios to estimate their chances

*axionahn@naver.com
†skkang@seoultech.ac.kr
‡rayramosang@gmail.com
§tanimoto@muse.sc.niigata-u.ac.jp

of survival in three long-baseline experiments that may be operative in the near future. We complete this work by showing how one of these scenarios can be realized in a flavor model of neutrino masses and mixing.

The rest of the paper is laid out as follows: In Sec. II we introduce the perturbations to TBM mixing that will be used in this work and their constraints on oscillation parameters. In Sec. III we present probability densities related to the CP-violating phase considering constraints from the cases of Sec. IIIn Sec. IV we describe the perturbed scenarios applied to BM mixing and comment on the effects of current experimental constraints. In Sec. V we present the prospects of future experiments expected to constrain the scenarios considered here. In Sec. VI we construct a model using A_4 modular symmetry that is consistent with one of the perturbed scenarios and expand on its properties. Finally, in Sec. VII we discuss the most relevant details of this work and conclude.

II. PERTURBATIVE MODIFICATIONS TO TRIBIMAXIMAL MIXING

Let us begin by recalling the form of the exact TBM mixing matrix [14]

$$U_0^{\rm TBM} = \begin{pmatrix} \sqrt{\frac{2}{3}} & \frac{1}{\sqrt{3}} & 0 \\ -\sqrt{\frac{1}{6}} & \frac{1}{\sqrt{3}} & \frac{1}{\sqrt{2}} \\ \sqrt{\frac{1}{6}} & -\frac{1}{\sqrt{3}} & \frac{1}{\sqrt{2}} \end{pmatrix}. \tag{1}$$

As mentioned before, this mixing matrix form has been the motivation for a great number of models that attempt to predict the neutrino oscillation parameters employing discrete symmetries. It is this sort of pattern with a vanishing 1–3 matrix element that were ruled out by the measurement of the nonzero reactor angle θ_{13}. In this paper we will consider the following minimal perturbations to the TBM mixing matrix:

$$V = \begin{cases} U_0^{\rm TBM} U_{23}(\theta,\phi) & (\text{Case A}), \\ U_0^{\rm TBM} U_{13}(\theta,\phi) & (\text{Case B}), \\ U_{12}^\dagger(\theta,\phi) U_0^{\rm TBM} & (\text{Case C}), \\ U_{13}^\dagger(\theta,\phi) U_0^{\rm TBM} & (\text{Case D}), \end{cases} \tag{2}$$

where the $U_{ij}(\theta,\phi)$ matrices are given by

$$U_{12}(\theta,\phi) = \begin{pmatrix} \cos\theta & -\sin\theta e^{i\phi} & 0 \\ \sin\theta e^{-i\phi} & \cos\theta & 0 \\ 0 & 0 & 1 \end{pmatrix}, \tag{3}$$

$$U_{13}(\theta,\phi) = \begin{pmatrix} \cos\theta & 0 & -\sin\theta e^{i\phi} \\ 0 & 1 & 0 \\ \sin\theta e^{-i\phi} & 0 & \cos\theta \end{pmatrix}, \tag{4}$$

$$U_{23}(\theta,\phi) = \begin{pmatrix} 1 & 0 & 0 \\ 0 & \cos\theta & -\sin\theta e^{i\phi} \\ 0 & \sin\theta e^{-i\phi} & \cos\theta \end{pmatrix}. \tag{5}$$

Finding the equivalence between the mixing matrix V of each case and the $U^{\rm PMNS}$ can be done elementwise with $V_{jk}\exp(i(\omega_j+\psi_k)) = U_{jk}^{\rm PMNS}\exp(i\varphi_k)$.

The exact TBM pattern of Eq. (1) can be regarded as the result of a residual symmetry in the charged lepton and neutrino sectors from a flavor model defined at a higher energy. In this case, the mixing matrices of cases A and B in Eq. (2) can be considered the consequence of additional effects that break this residual symmetry on the planes (2,3) and (1,3) in the side of the neutrino sector, respectively, leaving a residual Z_2 symmetry. Similarly, but on the side of the charged leptons, cases C and D would break the residual symmetry of the TBM pattern down to Z_2, resulting in additional rotations on the planes (1,2) and (1,3), respectively. Note that cases A and C were also studied in Refs. [41–43]. It is also worth noting that cases A and B are popularly known in the literature as trimaximal mixing 1 and 2 [25,44–48]. To simplify the notation, we will be using the shorthand $s_{ij} = \sin\theta_{ij}$ and $c_{ij} = \cos\theta_{ij}$ in the rest of the paper.

III. CP-VIOLATING PHASE FROM PERTURBATIVE SCENARIOS

One of the most relevant points of enabling a nonzero θ_{13} is opening up the possibility of having a Dirac-type CP-violating phase in the PMNS mixing matrix. Due to the features of the cases mentioned in Eq. (2) it is possible to relate either θ_{12} (cases A and B) or θ_{23} (cases C and D) with the reactor angle θ_{13} and, lastly, to relate the δ_{CP} phase to the pair of free mixing angles. This is achieved by identifying the parametrizations that result from Eq. (2) with the standard PDG parametrization of the PMNS matrix. In this way, in Ref. [18] the following relations between oscillation parameters were worked out:

$$\text{A:}\quad s_{12}^2 = 1 - \frac{2}{3(1-s_{13}^2)}, \qquad \cos\delta_{CP} = \frac{5s_{13}^2 - 1}{\eta_{23}s_{13}\sqrt{2-6s_{13}^2}}, \tag{6}$$

$$\text{B:}\quad s_{12}^2 = \frac{1}{3(1-s_{13}^2)}, \quad \cos\delta_{CP} = \frac{2-4s_{13}^2}{\eta_{23}s_{13}\sqrt{2-3s_{13}^2}}, \tag{7}$$

$$\text{C:}\quad s_{23}^2 = 1 - \frac{1}{2(1-s_{13}^2)},$$
$$\cos\delta_{CP} = \frac{s_{13}^2 - (1-3s_{12}^2)(1-3s_{13}^2)}{3s_{13}\xi\sqrt{1-2s_{13}^2}}, \tag{8}$$

$$\text{D:}\quad s_{23}^2 = \frac{1}{2(1-s_{13}^2)},$$
$$\cos\delta_{CP} = \frac{(1-3s_{12}^2)(1-3s_{13}^2) - s_{13}^2}{3s_{13}\xi\sqrt{1-2s_{13}^2}}, \tag{9}$$

where $\eta_{23} = 2\tan 2\theta_{23}$ and $\xi = \sin 2\theta_{12}$. Considering the form of the matrices of Eqs. (3)–(5) we can write the following expressions for the other oscillation parameters in terms of the angle θ and the phase ϕ:

$$\text{A:}\quad s_{13}^2 = \frac{\sin^2\theta}{3},\qquad s_{23}^2 = \frac{3-\sin^2\theta+\sqrt{6}\sin 2\theta\cos\phi}{6-2\sin^2\theta}, \tag{10}$$

$$\text{B:}\quad s_{13}^2 = \frac{2\sin^2\theta}{3},\qquad s_{23}^2 = \frac{3-2\sin^2\theta+\sqrt{3}\sin 2\theta\cos\phi}{6-4\sin^2\theta}, \tag{11}$$

$$\text{C, D:}\quad s_{13}^2 = \frac{\sin^2\theta}{2},\qquad s_{12}^2 = \frac{2}{3}\left(\frac{1-\sin 2\theta\cos\phi}{2-\sin^2\theta}\right), \tag{12}$$

Note that, for every case, there is a relationship between θ_{13} and θ, consistent with the idea that the matrices in Eqs. (3)–(5) are perturbations that deviate θ_{13} from zero. Using Eqs. (6)–(12), other noteworthy consequences of these perturbations include that for case A $s_{12}^2 < 1/3$, while for case B $s_{12}^2 > 1/3$, resulting in case B not being able to reproduce the current best fit value for this oscillation parameter. For cases C and D we obtain $s_{23}^2 < 1/2$ and $s_{23}^2 > 1/2$, respectively, meaning that whenever the octant of θ_{23} is resolved at least one of these two cases will be ruled out.

A. Probability densities of $\cos\delta_{CP}$

Using the expressions in Eqs. (6)–(9) and the measured oscillation parameters from NuFIT 5.1 global fit [49], we can calculate probability densities for the predictions of the δ_{CP} phase in every scenario. The process for calculating these densities follows Ref. [50]. There are three facts that simplify the process in the present case:

1. Considering $0 \le \sin^2\theta \le 1$, Eqs. (10)–(12) imply an upper bound on s_{13}^2 that completely contains the acceptable experimental range and, thus, has no relevant effect in this analysis.
2. With the same equations, the values we can get for s_{23}^2 in cases A and B are not particularly limited by specific values of s_{13}^2 in the range of interest from the global fit, therefore, we can consider s_{13}^2 independent of s_{23}^2.
3. Using input values around the 3σ range for s_{13}^2 and s_{23}^2 in cases A and B predicts only physical values for $\cos\delta_{CP}$.

Points 2 and 3 above are also true for cases C and D replacing s_{23}^2 by s_{12}^2. Considering these details, we can calculate the probability density for $\cos\delta_{CP}$ directly using the probability densities of s_{13}^2, s_{23}^2, and s_{12}^2. The integral that we have to perform to calculate the probability density at some particular value z of $\cos\delta_{CP}$ is given by

$$P^{(\mathrm{A,B})}_{\cos\delta_{CP}}(z) = \int dx\, dy\, \delta(f_{\mathrm{A,B}}(x,y) - z) P_{s_{13}^2}(x) P_{s_{23}^2}(y), \tag{13}$$

$$P^{(\mathrm{C,D})}_{\cos\delta_{CP}}(z) = \int dx\, dw\, \delta(f_{\mathrm{C,D}}(x,w) - z) P_{s_{13}^2}(x) P_{s_{12}^2}(w), \tag{14}$$

where w, x, y represent values of s_{12}^2, s_{13}^2, s_{23}^2, respectively, that we have to integrate over. The functions f_j, with $j \in \{\mathrm{A,B,C,D}\}$, represent $\cos\delta_{CP}$ for each case and the delta function ensures that the integration is performed over a line where $\cos\delta_{CP} = z$. Independently of the three points enumerated before, the probability densities $P_{s_{ij}^2}$ can be any

TABLE I. Oscillation parameters for three neutrino flavors as reported in NuFIT 5.1 [49] for normal ordering (NO) ($\Delta m_{3k}^2 = \Delta m_{31}^2$) and inverted ordering (IO) ($\Delta m_{3k}^2 = \Delta m_{32}^2$), including the tabulated χ^2 data from Super-Kamiokande.

Parameter	Best fit $\pm\,1\sigma$ (NO)	3σ range (NO)	Best fit $\pm\,1\sigma$ (IO)	3σ range (IO)
$\sin^2\theta_{12}$	0.304 ± 0.012	[0.269, 0.343]	$0.304^{+0.013}_{-0.012}$	[0.269, 0.343]
$\sin^2\theta_{13}$ $[10^{-2}]$	2.246 ± 0.062	[2.060, 2.435]	$2.241^{+0.074}_{-0.062}$	[2.055, 2.457]
$\sin^2\theta_{23}$	$0.450^{+0.019}_{-0.016}$	[0.408, 0.603]	$0.570^{+0.016}_{-0.022}$	[0.410, 0.613]
δ_{CP} [deg]	230^{+36}_{-25}	[144, 350]	278^{+22}_{-30}	[194, 345]
Δm_{21}^2 $[10^{-5}\ \mathrm{eV}^2]$	$7.42^{+0.21}_{-0.20}$	[6.82, 8.04]	$7.42^{+0.21}_{-0.20}$	[6.82, 8.04]
Δm_{3k}^2 $[10^{-3}\ \mathrm{eV}^2]$	2.510 ± 0.027	[2.430, 2.593]	$-2.490^{+0.26}_{-0.28}$	[−2.574, −2.410]

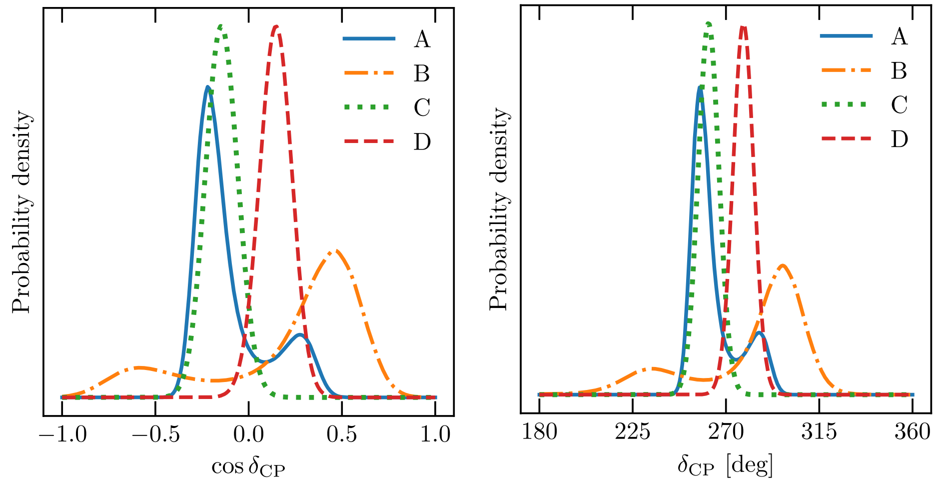

FIG. 1. Probability densities for $\cos\delta_{CP}$ (left) and δ_{CP} (right) using experimental results for normal ordering. The probability densities were obtained using the method detailed in Sec. III A and are normalized to one. The y-axis value is meaningless and does not indicate preference for any case; taller (shorter) densities indicate a more narrowly (widely) predicted $\cos\delta_{CP}$.

normalized function where the values of z are well defined in the integration intervals. Note that, in general, one of the two probability densities in each integral should be a conditional probability distribution dependent on the input of the other, however, given point 2 above, we are considering both distributions in each integral as independent.

For this work, we are interested in using Eqs. (13) and (14) to calculate $\cos\delta_{CP}$ probability densities from currently observed oscillation parameters. For this purpose we use the χ^2 tables provided by the NuFIT collaboration available on their website [51]. The data used corresponds to the normal (NO) and inverted (IO) ordering results that include Super-Kamiokande's tabulated χ^2 data (lower part of Table 3 in Ref. [49]), these have been collected in Table I for convenience. The χ^2 values are used to construct probability densities of the form $P(\alpha) = N\exp(-\chi^2(\alpha)/2)$, where $N = (\int d\alpha \exp(-\chi^2(\alpha)/2))^{-1}$ ensures that the probability density integrates to one. The probability densities obtained with the method described above are shown in Fig. 1 for $\cos\delta_{CP}$ and δ_{CP}. For cases A (blue line), C (green dotted line), and D (red dashed line), the prediction for $\cos\delta_{CP}$ lies inside the $[-0.5, 0.5]$ range, with case D mostly positive while case C is mostly negative. Case A has a more spread distribution but the most probable range for $\cos\delta_{CP}$ is predicted close to -0.25. The probability that corresponds to case B (orange dash-dotted line) is distributed along nearly all the $[-1, 1]$ range with its highest peak around 0.5. For the CP-violating phase δ_{CP} this means that A, C, and D are close to 90° or 270°.

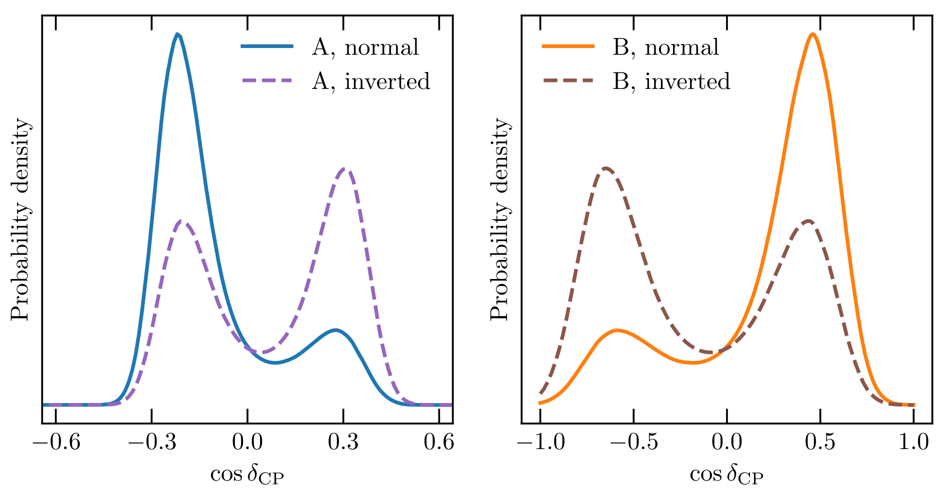

FIG. 2. Differences in the distribution of $\cos\delta_{CP}$ for cases A (left) and B (right) when considering data for NO (solid) and IO (dashed). The probability densities were obtained using the method detailed in Sec. III A and are normalized to one. The y-axis value is meaningless and does not indicate preference for any case; taller (shorter) densities indicate a more narrowly (widely) predicted $\cos\delta_{CP}$.

Note that the right side of Fig. 1 only shows the range $[180°, 360°]$, which is currently favored by observations. The range $(0, 180°)$ is just a mirror image of said figure.

The changes in the distributions of $\cos\delta_{CP}$ from considering NO or IO data from Table I is mostly related to changes in central values and χ^2 projections. Cases C and D, which depend on s_{13}^2 and s_{12}^2, do not change notably between using NO or IO data. However, in the case of A and B, due to the significant change in the χ^2 projection of s_{23}^2, the distribution of $\cos\delta_{CP}$ changes to display two more leveled peaks with the higher peak changing side in both cases. This can be seen in detail in Fig. 2, where we can see that for case A in IO (left pane, dashed line) the highest peak changes to ∼0.3 while for case B using IO data (right pane, dashed line) the highest peak moves to ~ -0.65. These changes can be interpreted as the delta *CP* phase δ_{CP} in case A changing from 256° in NO to 288° in IO, while for case B it changes from 297° in NO to 230° in IO.

IV. PERTURBATIVE MODIFICATIONS TO BIMAXIMAL MIXING

In the same way we modified the TBM mixing case in Sec. II, we can apply perturbations to the very well-known BM mixing [7–13]. The exact form of the BM mixing matrix is given by

$$U_0^{\rm BM} = \begin{pmatrix} \sqrt{\frac{1}{2}} & \frac{1}{\sqrt{2}} & 0 \\ -\frac{1}{2} & \frac{1}{2} & \frac{1}{\sqrt{2}} \\ \frac{1}{2} & -\frac{1}{2} & \frac{1}{\sqrt{2}} \end{pmatrix}. \tag{15}$$

From here, perturbations proceed identically as for the TBM case. We can define the following scenarios

$$V = \begin{cases} U_{12}^\dagger(\theta,\phi)U_0^{\rm BM} & \text{(Case E)}, \\ U_{13}^\dagger(\theta,\phi)U_0^{\rm BM} & \text{(Case F)}, \\ U_0^{\rm BM}U_{23}(\theta,\phi) & \text{(Case G)}, \\ U_0^{\rm BM}U_{13}(\theta,\phi) & \text{(Case H)}, \end{cases} \tag{16}$$

with the $U_{ij}(\theta,\phi)$ matrices given in Eqs. (3)–(5). Cases G and H were considered ruled out by experimental data above 3σ when they were studied on Ref. [18]. For cases E and F the expressions for s_{23}^2 are identical to those of cases C and D, respectively. The relationships between mixing angles and the *CP*-violating phase are given by

$$\text{E:}\quad \cos\delta_{CP} = \frac{3s_{13}^2 - 1}{\eta_{12}s_{13}\sqrt{1-2s_{13}^2}}, \tag{17}$$

$$\text{F:}\quad \cos\delta_{CP} = \frac{1 - 3s_{13}^2}{\eta_{12}s_{13}\sqrt{1-2s_{13}^2}}, \tag{18}$$

where $\eta_{12} = 2\tan 2\theta_{12}$.

To provide an update for cases E and F, we find that they cannot predict physical values for $\cos\delta_{CP}$ within the 3σ ranges using current results from Ref. [49]. In Fig. 3 the 3σ rectangles for s_{13}^2 and s_{12}^2 are shown together with the closer physical boundary (colored contours) for the predicted $\cos\delta_{CP}$ for both cases E and F. Interestingly, in both panes of Fig. 3, the boundary of the physical predictions for $\cos\delta_{CP}$ is barely outside the 3σ rectangle, almost touching the upper right corner, indicating that this level of exclusion must be quite recent.

With these results, all the cases with $U_0^{\rm BM}$ considered in Ref. [18] can be considered ruled out at 3σ or above. Considering this, we will not follow the detailed analysis of the previous section on the *CP*-violating Dirac phase for

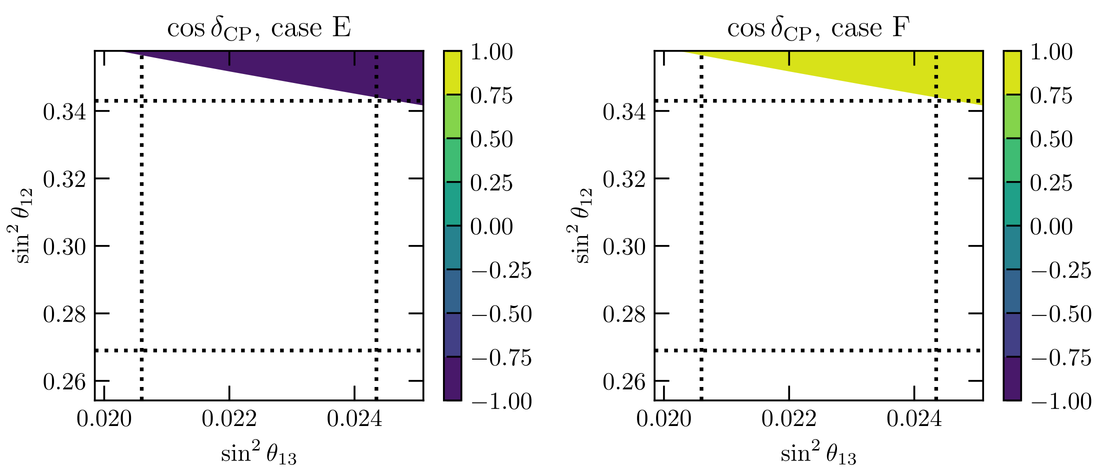

FIG. 3. Border of the physical region for $\cos\delta_{CP}$ closest to the $\pm 3\sigma$ rectangle for $s_{13}^2 - s_{12}^2$ (dotted lines). Predictions for $\cos\delta_{CP}$ use cases E (left) and F (right) from Ref. [18]. White regions indicate unphysical $\cos\delta_{CP}$.

the cases of this section and the rest of this work will be focused on cases A, B, C, and D.

V. PROSPECTS AT FUTURE EXPERIMENTS

To analyze the prospects for the four cases considered in this work, we will employ simulations using the GLoBES software package [52,53]. We will consider three long-baseline experiments: DUNE, T2HK, and ESSnuSB. For the DUNE experiment we consider the configuration detailed in their technical design report [54]. According to Ref. [54], the DUNE experiment is planned to have a long-baseline of 1300 km, with a 1.2 MW neutrino beam produced at Fermi National Accelerator Laboratory and received at a far detector in the Sanford Underground Research Facility. This corresponds to 1.1×10^{21} protons on target (POT). The far detector will consist of liquid argon time-projection chambers and will have a (fiducial) mass of (40 kt) 70 kt. In our simulation we assume a total run time of 7 years equally distributed between neutrino and antineutrino modes. In the case of the T2HK experiment we follow the setup described in Ref. [55]. A 1.3 MW neutrino beam will be produced at Japan Proton Accelerator Research Complex. The neutrinos would arrive to a water Cherenkov detector with a fiducial mass of 187 kt, at a distance of 295 km. A second identical detector is under consideration to be built in Korea. Assuming a total of 10 yr of operation of the first detector it is possible to achieve 27×10^{21} POT. Following Ref. [55], we assume that the 10 yr run time is distributed with a ratio of 3∶1 for antineutrino to neutrino modes. For ESSnuSB we consider the experimental setup outlined in Ref. [56]. The neutrino beam would be produced at the European Spallation Source with a power of 5 MW. Neutrinos would be received at a MEMPHYS-like [57] water Cherenkov detector with a (fiducial) mass of (507 kt) 1 Mt, at a distance of 540 km. With this configuration, ESSnuSB will reach 2.7×10^{23} POT per year. In our analysis, we assume a run of 10 yr with a ratio of 8∶2 for antineutrino to neutrino modes as mentioned in the "Nominal value" column of Table 1.1 of Ref. [56].

The statistical analysis follows the methodology described in Sec. III of Ref. [58]. To summarize the steps in this methodology, we start with GLoBES χ^2_{G} function comparing the N^{obs} events observed in the simulation of the experiment against N^{th} events expected from theory. GLoBES χ^2_G function can be written as

$$\chi^2_{\mathrm{G}}(\theta,\phi) = \sum_i \left[N_i^{\mathrm{th}}(\theta,\phi) - N_i^{\mathrm{obs}} + N_i^{\mathrm{obs}} \ln\left(\frac{N_i^{\mathrm{obs}}}{N_i^{\mathrm{th}}(\theta,\phi)} \right) \right], \tag{19}$$

where (θ,ϕ) refers to a set of parameters in the theory and the summation run over bins. Additionally, we include two Gaussian prior contributions to the total χ^2 using the reported central values, $s^2_{12,\mathrm{obs}}$ and $s^2_{13,\mathrm{obs}}$, and their respective 1σ errors, σ_{12} and σ_{23}, that can be read off from Table I [49]. Considering that currently the octant of s^2_{23} is not known, for its prior we use an interpolation of the χ^2 table provided in NuFIT's website [51]. The full χ^2_{pr} is given by

$$\chi^2_{\mathrm{pr}}(\theta,\phi) = \left(\frac{s^2_{12}(\theta,\phi) - s^2_{12,\mathrm{obs}}}{\sigma_{12}} \right)^2 + \left(\frac{s^2_{13}(\theta,\phi) - s^2_{13,\mathrm{obs}}}{\sigma_{13}} \right)^2 + \chi^2_{23,\mathrm{NuFIT}}(s^2_{23}(\theta,\phi)). \tag{20}$$

The total χ^2 to be minimized is given by

$$\chi^2(\theta,\phi) = \chi^2_{\mathrm{G}}(\theta,\phi) + \chi^2_{\mathrm{pr}}(\theta,\phi). \tag{21}$$

Following Ref. [58], our results will be presented for $\Delta\chi^2 = \chi^2_{\mathrm{mod}} - \chi^2_{\mathrm{free}}$, where χ^2_{mod} is the result of minimizing Eq. (21) over the model parameters θ and ϕ, while χ^2_{free} is the minimization over oscillation parameters ignoring constraints from the scenarios of Sec. II. For a similar analysis on DUNE and T2HK see Ref. [59], and for one on ESSnuSB see Ref. [60].

We performed scans over the true values in the plane $s^2_{23} - \delta_{CP}$, while fixing other true values to their central values, given in Table I. Note that, due to Eqs. (6) and (7), cases A and B cannot simultaneously have s^2_{12} and s^2_{13} at their current central values. This means that if an experiment or combination of experiments could measure the assumed true values $s^2_{12} = 0.304$ and $s^2_{13} = 0.02246$ with enough precision to reject any $s^2_{12} - s^2_{13}$ combination consistent with case A and/or B then that case would be rejected regardless of other parameters. Considering that cases A and B can always have $s^2_{13} = 0.02246$ the issue mostly concerns s^2_{12}. However, the experiments in our simulation are not expected to reduce the range of s^2_{12} enough to strongly constrain cases A and B, but have been chosen for their capacity to measure the δ_{CP} phase. The results of our simulations are presented in Fig. 4. One obvious feature is that cases C and D have a more constrained s^2_{23} compared to cases A and B. This is expected from the fact that, in cases C and D, s^2_{23} depends on the value of s^2_{13} which reduces its allowed range, while for cases A and B s^2_{23} is free. For cases C and D, the range of s^2_{23} is more strongly constrained by DUNE and T2HK, while for all cases ESSnuSB reduces the δ_{CP} phase range. Assuming that future experimental results will be close to the current best fit point (NO: red thick $\times$, IO: blue-white $+$), we can see that T2HK (red regions) alone could exclude cases C and D for both NO and IO at 5σ or more, while DUNE (blue regions) could exclude C and D only for the NO result, with the IO result remaining within 3 to 5σ. Under the same assumed future results, ESSnuSB could not exclude any case above 5σ. However, the combination of the three experiments (black contours) has the capacity of

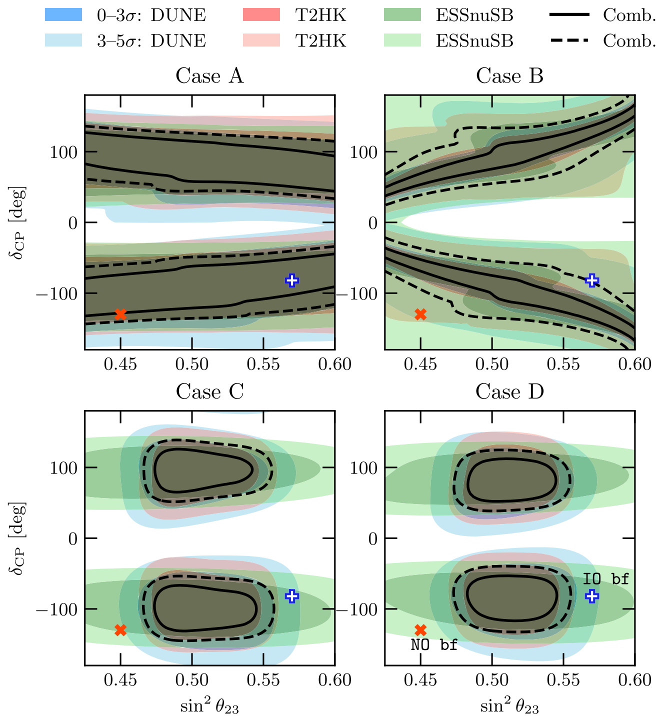

FIG. 4. Prospects of future experiments excluding cases A, B, C, and D in the plane $\sin^2\theta_{23} - \delta_{CP}$. A measurement in the white region (outside dashed black contour) indicates that the corresponding case could be excluded with 5σ or more confidence by the experiment (combined experiments). A measurement in the light colored region (between solid and dashed black contour) indicates an exclusion between 3σ to 5σ. If the experiment (combined experiments) measures a true value inside the darker region (solid black contour) then the result and the model are compatible within 3σ. The experimental results used in the simulation correspond to normal ordering, however, there is no significant change for inverted ordering other than the current best fit point, indicated as a red thick × for NO and a blue-white + for IO.

excluding cases B, C, and D for both orderings to 5σ or more. Case A has the best chances of survival, with a NO result disfavoured only between 3 to 5σ and IO staying well below 3σ.

Here we point out that the results from Sec. III A are product of considering current measured oscillation parameters on Eqs. (6)–(9) while the results of this section represent prospects of future experimental measurements being compatible (or incompatible) with the constraints of the same equations. Interestingly, we see that some features regarding the displayed ranges of $\cos\delta_{CP}$ are shared between them. For example, in both Figs. 1 and 4 cases A and B have broader ranges for the *CP* violating phase δ_{CP} while cases C and D have somewhat narrower ranges for the same. Another interesting point is that, if future experiments could resolve the θ_{23} octant, cases A and B would more strongly prefer opposite sign $\cos\delta_{CP}$. With $\theta_{23} < 0.5$ case A would prefer negative $\cos\delta_{CP}$ while B would mostly fall positive. In the situation where θ_{23} would be resolved above 0.5 then case A would go positive while case B would prefer negative. This can be seen in the top panels of Fig. 4 and would result in $\cos\delta_{CP}$ distributions for cases A and B peaking towards their corresponding preferred values in Figs. 1 and 2.

VI. A MODEL WITH A_4 MODULAR SYMMETRY

In this section we will construct a model that predicts the neutrino masses and mixing within the measured limits, and we will show that symmetry breaking in this model results in a mixing pattern that is consistent with case A studied in previous sections. In the context of modular symmetries, other works have also obtained the TM_1 mixing pattern that matches case A [61–63].

The properties of modular forms are described in detail in Ref. [64]. To summarize the modular approach to flavor models, consider the group $\Gamma(N)$ defined by

$$\Gamma(N) = \left\{ \begin{pmatrix} a & b \\ c & d \end{pmatrix} \in SL(2,Z), \begin{pmatrix} a & b \\ c & d \end{pmatrix} = \begin{pmatrix} 1 & 0 \\ 0 & 1 \end{pmatrix} \pmod N \right\}, \tag{22}$$

where $SL(2,Z)$ is the special linear group of 2×2 matrices with integer elements and determinant equal to 1. The elements of the group $\Gamma(N)$ transform a complex variable τ, constrained by $\mathrm{Im}(\tau) > 0$, according to

$$\gamma\tau = \frac{a\tau + b}{c\tau + d} \tag{23}$$

we call this a linear fractional transformation. The group of these linear fractional transformations, represented by $\bar\Gamma(N)$, is related to $\Gamma(N)$: for $N \le 2$, $\bar\Gamma(N) \equiv \Gamma(N)/\{\pm\mathbb{1}\}$, while for $N > 2$ we have $\bar\Gamma(N) \equiv \Gamma(N)$. For $N = 1$ we can write $\bar\Gamma \equiv \bar\Gamma(1)$. The generators of the group $\bar\Gamma$ can be expressed using the $SL(2,Z)$ matrices

$$S = \begin{pmatrix} 0 & -1 \\ 1 & 0 \end{pmatrix}, \qquad T = \begin{pmatrix} 1 & 1 \\ 0 & 1 \end{pmatrix}, \tag{24}$$

which satisfy the relation $S^2 = (ST)^3 = \mathbb{1}$. The quotient $\bar\Gamma/\bar\Gamma(N)$ defines finite groups referred as finite modulars groups Γ_N. The generators of these groups have the additional property that $T^N = \mathbb{1}$. For $N \in \{2,3,4,5\}$ these groups are isomorphic to the permutation groups S_3, A_4, S_4, and A_5, respectively. For further details on modular forms and their relation to the permutation groups mentioned, the interested reader may check Refs. [63–67].

The model that we develop here is based on modular forms of level $N = 3$ which have a quotient group, Γ_3, isomorphic to A_4, the symmetry group of the tetrahedron. For A_4 the generators have the properties

$$S^2 = (ST)^3 = T^3 = \mathbb{1}. \quad (25)$$

The modular forms of level 3 were constructed on Appendix C of Ref. [64] and correspond to

$$Y_1(\tau) = \frac{i}{2\pi}\left[\frac{\eta'(\frac{\tau}{3})}{\eta(\frac{\tau}{3})} + \frac{\eta'(\frac{\tau+1}{3})}{\eta(\frac{\tau+1}{3})} + \frac{\eta'(\frac{\tau+2}{3})}{\eta(\frac{\tau+2}{3})} - \frac{27\eta'(3\tau)}{\eta(3\tau)}\right],$$
$$Y_2(\tau) = \frac{-i}{\pi}\left[\frac{\eta'(\frac{\tau}{3})}{\eta(\frac{\tau}{3})} + \omega^2\frac{\eta'(\frac{\tau+1}{3})}{\eta(\frac{\tau+1}{3})} + \omega\frac{\eta'(\frac{\tau+2}{3})}{\eta(\frac{\tau+2}{3})}\right],$$
$$Y_3(\tau) = \frac{-i}{\pi}\left[\frac{\eta'(\frac{\tau}{3})}{\eta(\frac{\tau}{3})} + \omega\frac{\eta'(\frac{\tau+1}{3})}{\eta(\frac{\tau+1}{3})} + \omega^2\frac{\eta'(\frac{\tau+2}{3})}{\eta(\frac{\tau+2}{3})}\right], \quad (26)$$

where η is the Dedekind eta function defined by

$$\eta(\tau) = q^{1/24}\prod_{n=1}^{\infty}(1-q^n), \qquad q \equiv \exp(i2\pi\tau), \qquad \mathrm{Im}(\tau) > 0, \quad (27)$$

and $\omega = (-1+i\sqrt{3})/2$. The forms Y_i belong to an A_4 triplet $(Y_1, Y_2, Y_3) \equiv Y$.

A. Lepton masses

We will consider Majorana neutrinos that acquire small masses via the seesaw mechanism. This model is based on an extension by the symmetry group $A_4 \times U(1)_X$ with the right-handed neutrinos in a triplet of chiral supermultiplets N^c. The field content of the model, A_4 representation, $U(1)_X$ charges, and modular weights k_I are collected in Table II. With those assignments for the fields, the superpotential is given by

$$W = \alpha_1 e^c L_e Y_{\mathbf{1}}^{(6)}\left(\frac{\chi}{\Lambda}\right)^{f_e} H_d + \alpha_2 \mu^c L_\mu Y_{\mathbf{1}}^{(6)}\left(\frac{\chi}{\Lambda}\right)^{f_\mu} H_d + \alpha_3 \tau^c L_\tau Y_{\mathbf{1}}^{(6)}\left(\frac{\chi}{\Lambda}\right)^{f_\tau} H_d + \beta_1 (N^c Y)_{\mathbf{1}} L_e H_u + \beta_2 (N^c Y)_{\mathbf{1}''} L_\mu H_u$$
$$+ \beta_3 (N^c Y)_{\mathbf{1}'} L_\tau H_u + \gamma_1 (N^c N^c)_{\mathbf{1}} Y_{\mathbf{1}}^{(4)}\chi + \gamma_2 (N^c N^c)_{\mathbf{3}} Y_{\mathbf{3}}^{(4)}\chi + \gamma_3 (N^c N^c)_{\mathbf{1}''} Y_{\mathbf{1}'}^{(4)}\chi, \quad (28)$$

where α_i, β_i and γ_i are dimensionless couplings. Higher order terms are possible but are expected to be heavily suppressed. Imposing CP symmetry in the compactification scale, the α_i, β_i, and γ_i are made real and are taken as $\mathcal{O}(1)$ coefficients [66]. The weights 4 and 6 modular forms used above are given by

$$Y_{\mathbf{1}}^{(4)} = Y_1^2 + 2Y_2Y_3, \quad (29)$$

$$Y_{\mathbf{1}'}^{(4)} = Y_3^2 + 2Y_1Y_2, \quad (30)$$

$$Y_{\mathbf{3}}^{(4)} = (Y_1^2 - Y_2Y_3, Y_3^2 - Y_1Y_2, Y_2^2 - Y_1Y_3), \quad (31)$$

$$Y_{\mathbf{1}}^{(6)} = Y_1^3 + Y_2^3 + Y_3^3 - 3Y_1Y_2Y_3. \quad (32)$$

When the scalars, χ, H_u, and H_d, have acquired vacuum expectation value (VEV) the fields in the superpotential of Eq. (28) receive masses. While χ should be expected to acquire a large VEV at a high energy scale, H_u and H_d acquire VEVs at energies below the electroweak scale. The charged lepton masses can be extracted from the first line of the superpotential and correspond to the diagonal matrix

$$\mathcal{M}_\ell = Y_1^3\langle H_d\rangle(1 + a^3 + b^3 - 3ab)$$
$$\times \mathrm{diag}\left(\alpha_1\left(\frac{\langle\chi\rangle}{\Lambda}\right)^{f_e}, \alpha_2\left(\frac{\langle\chi\rangle}{\Lambda}\right)^{f_\mu}, \alpha_3\left(\frac{\langle\chi\rangle}{\Lambda}\right)^{f_\tau}\right), \quad (33)$$

where $a \equiv Y_2/Y_1$ and $b \equiv Y_3/Y_1$. One can choose integers $f_{e,\mu,\tau}$ and $\langle\chi\rangle/\Lambda$ in order for $(\langle\chi\rangle/\Lambda)^{f_e - f_\tau} = 0.0003$ and $(\langle\chi\rangle/\Lambda)^{f_\mu - f_\tau} = 0.06$ to satisfy the empirical results of charged lepton masses. From the second and third lines in the superpotential we can read off the following mass matrices

TABLE II. Fields of the model, their representation under the symmetries considered, and modular weights k_I.

	e^c,	μ^c,	τ^c	N^c	L_e,	L_μ,	L_τ	H_d	H_u	χ
$SU(2)_L \times U(1)_Y$		$(1, +1)$		$(1,0)$		$(2, -1/2)$		$(2, -1/2)$	$(2, +1/2)$	$(1,0)$
A_4	$\mathbf{1}$,	$\mathbf{1}''$,	$\mathbf{1}'$	3	1,	$\mathbf{1}'$,	$\mathbf{1}''$	$\mathbf{1}$	$\mathbf{1}$	$\mathbf{1}$
$U(1)_X$	$-\frac{1}{2} - f_e$,	$-\frac{1}{2} - f_\mu$,	$-\frac{1}{2} - f_\tau$	$-\frac{1}{2}$		$\frac{1}{2}$		0	0	1
k_I		6		2		0		0	0	0

$$m_D = Y_1 \langle H_u \rangle \beta_1 \begin{pmatrix} 1 & \beta b & \beta' a \\ b & \beta a & \beta' \\ a & \beta & \beta' b \end{pmatrix}, \tag{34}$$

$$M_R = Y_1^2 \langle \chi \rangle \gamma_1 \begin{pmatrix} 1 + \frac{4}{3}\gamma + ab(2 - \frac{4}{3}\gamma) & 2\gamma b & -\frac{2}{3}\gamma(b^2 - a) + \gamma'(b^2 + 2a) \\ (M_R)_{1,2} & \frac{4}{3}\gamma(b^2 - a) + \gamma'(b^2 + 2a) & 1 - \frac{2}{3}\gamma + ab(2 + \frac{2}{3}\gamma) \\ (M_R)_{1,3} & (M_R)_{2,3} & -4\gamma b \end{pmatrix}, \tag{35}$$

respectively, with $\beta \equiv \beta_2/\beta_1$, $\beta' \equiv \beta_3/\beta_1$, $\gamma \equiv \gamma_2/\gamma_1$, and $\gamma' \equiv \gamma_3/\gamma_1$. The matrix m_D corresponds to the Dirac masses for the neutrinos and the symmetric matrix M_R is for the Majorana masses of the right-handed neutrinos. From these matrices we obtain the light neutrino mass matrix

$$\mathcal{M}_\nu = -m_D^T M_R^{-1} m_D. \tag{36}$$

Note that the light mass matrix is proportional to $\langle H_u \rangle^2 / \langle \chi \rangle$, therefore, neutrino masses are expected to be small for very large $\langle \chi \rangle$.

Since the A_4 flavor models of leptons give large flavor mixing angles clearly [68,69], several A_4 modular invariant models have been proposed (see, e.g., [70–91]). It may be useful to comment on the distinctive features of our model. Our charged lepton mass matrix is diagonal, in contrast to previous models, by assignment of A_4 singlets for both left-handed and right-handed leptons apart from the right-handed neutrinos. Then, the lepton mixing angles come from flavor structure of the neutrino mass matrices. Therefore, our model is advantageous for discussing the TBM and the case A in the context of A_4 flavor symmetry. It is emphasized that in our model leptonic Dirac *CP* violation comes from the real part of τ since it is the only complex valued parameter in Eqs. (34) and (35). In fact, as we will see later, the Dirac *CP* violating phase $\delta_{CP} \approx 3\pi/2$ can be reproduced for $\mathrm{Re}(\tau) \approx 0.28$.

B. Perturbative modifications to TBM mixing

As mentioned in Sec. II, in the cases where the perturbation to TBM mixing is due to the breaking of residual symmetries in the neutrinos sector, such as the model presented here, we can expect perturbations of the form of cases A or B.

Considering the constraint imposed on s_{12}^2, mentioned before the start of Sec. III A, case B is unable to reproduce the current best fit value for s_{12}^2. This leaves case A as the most appropriate candidate for realistic phenomenological studies. Here we will attempt to show that the A_4 model presented above can predict oscillation parameters that are consistent with case A and are in complete agreement with the current best fit limits summarized in Table I.

As a first step, we find a few parameter choices that give predictions with good agreement with current experimental values and are consistent with case A, characterized by Eq. (6). We provide a few benchmark points in Table III labeled as Aj as well as their predictions in Table IVİn all the benchmark points, the overall factor of $\mathcal{M}_\nu$ is taken as $\langle H_u \rangle^2 \beta_1^2 / \langle \chi \rangle \gamma_1 = 5.4572 \times 10^{-12}$ GeV. The next step is finding a neighboring point that reproduces TBM with good accuracy. Such a point should be considered only illustrative, since TBM is in disagreement with current bounds, namely, with the measured range for s_{13}^2. The TBM point for our A_4 model is given in Table III with the label TBM. Then, we can compare these two types of points to assess how much each parameter changes between TBM and the perturbed case A.

First, recall that due to $s_{13}^2 = 0$ in the TBM mixing there is no *CP* violating phase. In our A_4 model, the source of *CP* violation in the matrices of Eqs. (34) and (35) is the complex values of the ratios of modular forms, a and b. Therefore, in the TBM mixing we can expect the τ parameter to be completely imaginary making a and b real. In fact, we find that we can repeat the TBM mixing

TABLE III. Benchmark points for the model presented in Sec. VI that predict a pattern consistent with case A and a neighboring point that predicts TBM mixing. A0 is the best fit point in the model consistent with case A.

	τ	β	β'	γ	γ'
A0	$0.28303 + i0.98882$	−1.6850	2.1293	0.27850	0.23788
A1	$0.27859 + i0.98630$	−1.7191	2.2104	0.26016	0.25510
A2	$0.28491 + i0.99292$	−1.6562	2.0412	0.30203	0.22781
A3	$0.28747 + i0.99414$	−1.6288	1.9900	0.31567	0.21780
TBM	i	−2.0	2.0	Free	1.0

TABLE IV. Predictions for the oscillation parameters using the corresponding point from Table III. The values of s_{13}^2, s_{23}^2, Δm_{21}^2, and Δm_{31}^2 are inside their 1σ ranges as given in Table I, $\sum m_\nu$ is below the cosmological upper bound of 0.12 eV. The values of s_{12}^2 and $\cos\delta_{CP}$ follow Eq. (6).

	s_{12}^2	s_{13}^2	s_{23}^2	$\cos\delta_{CP}$	Δm_{21}^2 [eV^2]	Δm_{31}^2 [eV^2]	$m_{\nu 1}$ [eV]	$\sum m_\nu$ [eV]
A0	0.3180	0.02249	0.4482	−0.2258	7.423	2.510	0.009017	0.07239
A1	0.3183	0.02210	0.4370	−0.2780	7.282	2.499	0.009432	0.07303
A2	0.3184	0.02191	0.4629	−0.1637	7.418	2.502	0.008453	0.07125
A3	0.3180	0.02242	0.4674	−0.1419	7.241	2.519	0.008203	0.07088

pattern for the fixed point $\tau = i$, where the $Z_2 = \{S, I\}$ subgroup of A_4 is preserved [63].[1] It is also well known that the TBM mixing implies a symmetry between ν_μ and ν_τ, therefore, we should expect this symmetry to appear in the matrix of Eq. (34). When comparing the points in Table III we see that β' and $\mathrm{Im}(\tau)$ change the least, with $\mathrm{Im}(\tau)$ matching at least two significant digits when going from Aj to TBM benchmark points. The parameters γ' and $\mathrm{Re}(\tau)$ change the most, with $\gamma' \approx 1$ for the TBM pattern which is 4 to 5 times the value in Aj. Considering that the complex τ parameters is the source of CP violation, it is understandable that it changes notably from the TBM case where CP violation is absent due to $s_{13}^2 = 0$. We find that for the TBM benchmark point $|\beta| = |\beta'|$, while in all the Aj points these two parameters only remain close in size. Close inspection of Eq. (34) reveals that β and β' are couplings related to μ and τ families and we can interpret their closesness in absolute value as related to the $\mu - \tau$ symmetry. More details about the $\tau = i$ limit and the TBM benchmark point are given in the Appendix.

The total number of free parameters in our scan is six: the real and imaginary part of $\tau, \beta, \beta', \gamma$, and γ'. We also have an overall factor that we can use to adjust the mass scale of the neutrinos. This overall factor facilitates predicting a neutrino mass sum that is well bellow the current cosmological upper bound of 0.12 eV [92]. Using these parameters we can make predictions for the 3 mixing angles and the CP-violating phase of the PMNS mixing matrix, the two neutrino squared mass differences and the mass of the lightest neutrino. The predictions for the Aj benchmark points of Table III are shown in Table IV. We choose points that predict s_{13}^2, s_{23}^2, Δm_{21}^2, and Δm_{31}^2 within 1σ of the values in Table I. The predictions for the masses of the neutrinos are consistent with squared mass differences for the normal ordering. The values of s_{12}^2 and $\cos\delta_{CP}$ follow the expressions of Eq. (6). Note that the values for $\cos\delta_{CP}$ in Table IV can be compared with the left panel of Fig. 1 and are found in the interval with the highest probability density.

[1]Note that at $\tau = i$, $Y_1^{(6)}$ vanishes and, then, charged leptons would be massless. In the Appendix we show more details about the $\tau = i$ and the TBM mixing limits.

It is important to mention that, while the TBM benchmark point of Table III corresponds to $\mathcal{M}_\nu$ diagonalizable by Eq. (1), the benchmark points Aj do not automatically result in $\mathcal{M}_\nu$ being diagonalized by matrices of the form $U_0^{\mathrm{TBM}} U_{23}(\theta, \phi)$. However, what one would observe instead, is that the absolute value of the elements in the first column of the PMNS matrix between the TBM and Aj benchmark points would not change. In general, the diagonalization of $\mathcal{M}_\nu$ employs a matrix whose elements can be parametrized as $V_{jk} \exp(i(\omega_j + \psi_k))$ with $j, k = 1, 2, 3$. The expressions from Sec. III were obtained by comparing these elements against the elements of the standard PDG parametrization of the leptonig mixing matrix [18]. For case A, after extracting the $\exp(i(\omega_j + \psi_k))$ part, we are left with $V = U_0^{\mathrm{TBM}} U_{23}(\theta, \phi)$, i.e., a matrix that keeps the first column of U_0^{TBM} unchanged.

To conclude this section with a comment, while the A_4 model presented above permits mixing patterns far more complicated, the study of this section illustrates how case A may arise in a realistic model. Moreover, the relation that exists between case A and TBM mixing is made explicit in the comparison between model parameter values. This analysis is independent of the model and could be a starting point for a detailed study of the effects of breaking the residual symmetries that led to TBM mixing in the first place.

VII. CONCLUSION

In this work we revisit the perturbed mixing patterns that were considered in Ref. [18] for the popular BM and TBM mixings. Using current best fit values and 3σ ranges for the oscillation parameters we found that the considered perturbations to BM mixing, labeled E and F, cannot predict physical values for $\cos\delta_{CP}$ with s_{12}^2 and s_{13}^2 inside their 3σ ranges, while the four cases that consider perturbations of TBM mixing survived. We extended on previous efforts to predict the leptonic CP-violating Dirac phase by calculating distributions for its allowed values in light of the relations between oscillations parameters. For cases A, B and C we found that the preferred δ_{CP} phase is located around 270° while for case B the most favoured values spanned a range roughly from 200° to 320°. These values consider that, according to Ref. [49], the observed preferred range for δ_{CP} is between 144° and 350°. Interestingly, planned experiments will have the power to constrain these simple perturbations, particularly cases B, C and D, which have the most constraining conditions. In the case of B, $s_{12}^2 > 1/3$ is in tension with the currently measured value, and if future experiments keep this tendency we will see the tension increased. For cases C and D, due to each case predicting s_{23}^2 in different octants, one of them will be excluded when the octant problem is resolved. Nonetheless, both cases, C and D, predict s_{23}^2 quite close to $1/2$, and if s_{23}^2 stays in close proximity to its current central value both cases could eventually be ruled out. The simulations performed and described in Sec. V show that DUNE, T2HK, and ESSnuSB experiments have the combined capacity to rule out cases B, C, and D by more than 5σ, while case A could be left disfavored by more than 3σ, when the future best fit value is assumed close to the current one. Interestingly, we can see hints from the probability intervals calculated in Sec. III A in the experimental expectations, most notably concerning the ranges for δ_{CP}. We finalize by showing the emergence of case A from an A_4 modular symmetry flavor model. This model is capable of predicting currently measured oscillation parameters within their acceptable ranges. Moreover, we showed that the model can predict TBM mixing and compare with points consistent with case A to illustrate the degree of perturbation required in the parameters. The results of this study can be applied to any model that results in a mixing pattern consistent with the list in Eq. (2). Furthermore, any of the steps performed in this study could be applied to different neutrino masses and mixing models for which one can obtain relations like those in Eqs. (6)–(9), and may help reveal details brought about by the existence of such constraints.

ACKNOWLEDGMENTS

Y. H. A. was supported by the National Research Foundation of Korea (NRF) grant funded by the Korea government (MSIT) (No. 2020R1A2C1010617). S. K. K. was supported by the National Research Foundation of Korea (NRF) grant funded by the Korea government (MSIT) (No. 2019R1A2C1088953). R. R. was supported by the National Research Foundation of Korea (NRF) grant funded by the Korea government (MSIT) (No. 2021R1A2C4002551).

APPENDIX: THE A_4 MODULAR SYMMETRY MODEL IN THE $\tau = i$ LIMIT

The A_4 model of Sec. VI can repeat the TBM mixing pattern in the limit $\tau = i$. There are several problems with this limit, most importantly, the $Y_{\mathbf{1}}^{(6)}$ modular form is zero resulting in massless charged leptons due to Eq. (33). However, here we want to take $\tau = i$ as an illustrative point on how this A_4 model goes from TBM mixing to the more experimentally conforming case A. In the limit $\tau = i$, the terms of the symmetric neutrino mass matrix take the form

$$[\mathcal{M}_\nu(\tau = i)]_{(1,1)} = \xi(-4\gamma + 3\gamma' + 3), \qquad \text{(A1)}$$

$$[\mathcal{M}_\nu(\tau = i)]_{(1,2)} = \xi\beta(2\gamma - 3\gamma'), \qquad \text{(A2)}$$

$$[\mathcal{M}_\nu(\tau = i)]_{(1,3)} = \xi\beta'(2\gamma - 3), \qquad \text{(A3)}$$

$$[\mathcal{M}_\nu(\tau = i)]_{(2,2)} = \xi\beta^2(-4\gamma - 3), \qquad \text{(A4)}$$

$$[\mathcal{M}_\nu(\tau = i)]_{(2,3)} = \xi\beta\beta'(2\gamma + 3\gamma' + 3), \qquad \text{(A5)}$$

$$[\mathcal{M}_\nu(\tau = i)]_{(3,3)} = \xi\beta'^2(-4\gamma - 3\gamma'), \qquad \text{(A6)}$$

where $\xi = \langle H_u\rangle^2\beta_1^2/[\langle\chi\rangle\gamma_1(4\gamma^2 - 3\gamma'^2 - 3\gamma' - 3)]$. The first detail to note here is that if $\gamma' = 1$ and $|\beta| = |\beta'|$ then we have $|(\mathcal{M}_\nu)_{(1,2)}| = |(\mathcal{M}_\nu)_{(1,3)}|$ and $|(\mathcal{M}_\nu)_{(2,2)}| = |(\mathcal{M}_\nu)_{(3,3)}|$. With this choices we have fixed $s_{13}^2 = 0$ and $s_{23}^2 = 0.5$. The remaining oscillation angle, θ_{12}, is now given by $s_{12}^2 = 2/(|\beta|^2 + 2)$, which gives $1/3$ if $|\beta| = 2$. In fact, the choice of parameter values of the TBM benchmark point given in Table III repeats Eq. (1) exactly.

Regarding neutrino masses, just by taking the limit $\tau = i$, one of the neutrinos becomes massless, demonstrated by the vanishing determinant of $\mathcal{M}_\nu(\tau = i)$. Moreover, taking the parameters as indicated in the previous paragraph, one can obtain the neutrino mass eigenstates with masses

$$m_{\nu 2} = -\frac{\langle H_u\rangle^2\beta_1^2}{\langle\chi\rangle\gamma_1}\frac{6}{2\gamma + 3}, \qquad \text{(A7)}$$

$$m_{\nu 3} = -\frac{\langle H_u\rangle^2\beta_1^2}{\langle\chi\rangle\gamma_1}\frac{12}{2\gamma - 3}. \qquad \text{(A8)}$$

For the TBM benchmark point given in Table III, we skipped testing for mass differences and cosmological bound since it is only an illustrative point for where TBM mixing is found. However, the perturbations discussed in Sec. VI, as illustrated by the benchmark points of Table III, can predict oscillation parameters and lepton masses that are consistent with current experimental constraints and the conditions of case A, as can be verified with the numbers of Table IV.

[1] Y. Fukuda *et al.* (Super-Kamiokande Collaboration), Evidence for Oscillation of Atmospheric Neutrinos, Phys. Rev. Lett. **81**, 1562 (1998).
[2] Q. R. Ahmad *et al.* (SNO Collaboration), Measurement of the Rate of $\nu_e + d \to p + p + e^-$ Interactions Produced by ^{8}B Solar Neutrinos at the Sudbury Neutrino Observatory, Phys. Rev. Lett. **87**, 071301 (2001).
[3] Y. Abe *et al.* (Double Chooz Collaboration), Indication of Reactor $\bar{\nu}_e$ Disappearance in the Double Chooz Experiment, Phys. Rev. Lett. **108**, 131801 (2012).
[4] F. P. An *et al.* (Daya Bay Collaboration), Observation of Electron-Antineutrino Disappearance at Daya Bay, Phys. Rev. Lett. **108**, 171803 (2012).
[5] B. Pontecorvo, Mesonium and anti-mesonium, Sov. Phys. JETP **6**, 429 (1957).
[6] Z. Maki, M. Nakagawa, and S. Sakata, Remarks on the unified model of elementary particles, Prog. Theor. Phys. **28**, 870 (1962).
[7] F. Vissani, A study of the scenario with nearly degenerate Majorana neutrinos, arXiv:hep-ph/9708483.
[8] V. D. Barger, S. Pakvasa, T. J. Weiler, and K. Whisnant, Bimaximal mixing of three neutrinos, Phys. Lett. B **437**, 107 (1998).
[9] A. J. Baltz, A. S. Goldhaber, and M. Goldhaber, The Solar Neutrino Puzzle: An Oscillation Solution with Maximal Neutrino Mixing, Phys. Rev. Lett. **81**, 5730 (1998).
[10] H. Fritzsch and Z. z. Xing, Large leptonic flavor mixing and the mass spectrum of leptons, Phys. Lett. B **440**, 313 (1998).
[11] R. N. Mohapatra and S. Nussinov, Gauge model for bimaximal neutrino mixing, Phys. Lett. B **441**, 299 (1998).
[12] S. K. Kang and C. S. Kim, Bimaximal lepton flavor mixing matrix and neutrino oscillation, Phys. Rev. D **59**, 091302 (1999).
[13] G. Altarelli, F. Feruglio, and L. Merlo, Revisiting bimaximal neutrino mixing in a model with S(4) discrete symmetry, J. High Energy Phys. 05 (2009) 020.
[14] P. F. Harrison, D. H. Perkins, and W. G. Scott, Tri-bimaximal mixing and the neutrino oscillation data, Phys. Lett. B **530**, 167 (2002).
[15] P. F. Harrison and W. G. Scott, Symmetries and generalizations of tri-bimaximal neutrino mixing, Phys. Lett. B **535**, 163 (2002).
[16] Z. z. Xing, H. Zhang, and S. Zhou, Nearly tri-bimaximal neutrino mixing and *CP* violation from mu-tau symmetry breaking, Phys. Lett. B **641**, 189 (2006).
[17] X. G. He and A. Zee, Some simple mixing and mass matrices for neutrinos, Phys. Lett. B **560**, 87 (2003).
[18] S. K. Kang and C. S. Kim, Prediction of leptonic *CP* phase from perturbatively modified tribimaximal (or bimaximal) mixing, Phys. Rev. D **90**, 077301 (2014).
[19] S. K. Kang, C. S. Kim, and J. D. Kim, Neutrino masses and leptonic *CP* violation, Phys. Rev. D **62**, 073011 (2000).
[20] M. Fukugita and M. Tanimoto, Lepton flavor mixing matrix and *CP* violation from neutrino oscillation experiments, Phys. Lett. B **515**, 30 (2001).
[21] C. Giunti and M. Tanimoto, *CP* violation in bilarge lepton mixing, Phys. Rev. D **66**, 113006 (2002).
[22] Z. z. Xing, Nearly tri bimaximal neutrino mixing and *CP* violation, Phys. Lett. B **533**, 85 (2002).
[23] W. l. Guo and Z. z. Xing, Calculable *CP* violating phases in the minimal seesaw model of leptogenesis and neutrino mixing, Phys. Lett. B **583**, 163 (2004).
[24] S. T. Petcov and W. Rodejohann, Flavor symmetry $L_e - L_\mu - L\tau$, atmospheric neutrino mixing and *CP* violation in the lepton sector, Phys. Rev. D **71**, 073002 (2005).
[25] C. H. Albright and W. Rodejohann, Comparing trimaximal mixing and its variants with deviations from tri-bimaximal mixing, Eur. Phys. J. C **62**, 599 (2009).
[26] W. Grimus and L. Lavoura, A model for trimaximal lepton mixing, J. High Energy Phys. 09 (2008) 106.
[27] S. F. Ge, D. A. Dicus, and W. W. Repko, $\mathbb{Z}_2$ symmetry prediction for the leptonic dirac *CP* phase, Phys. Lett. B **702**, 220 (2011).
[28] D. Marzocca, S. T. Petcov, A. Romanino, and M. Spinrath, Sizeable θ_{13} from the charged lepton sector in SU(5), (tri-) bimaximal neutrino mixing and dirac *CP* violation, J. High Energy Phys. 11 (2011) 009.
[29] H. J. He and F. R. Yin, Common origin of $\mu - \tau$ and *CP* breaking in neutrino seesaw, baryon asymmetry, and hidden flavor symmetry, Phys. Rev. D **84**, 033009 (2011).
[30] Y. Shimizu, M. Tanimoto, and K. Yamamoto, Predicting *CP* violation in deviation from tri-bimaximal mixing of neutrinos, Mod. Phys. Lett. A **30**, 1550002 (2015).
[31] S. T. Petcov, Predicting the values of the leptonic *CP* violation phases in theories with discrete flavour symmetries, Nucl. Phys. **B892**, 400 (2015).
[32] I. Girardi, S. T. Petcov, and A. V. Titov, Determining the dirac *CP* violation phase in the neutrino mixing matrix from sum rules, Nucl. Phys. **B894**, 733 (2015).
[33] S. K. Kang and M. Tanimoto, Prediction of leptonic *CP* phase in A_4 symmetric model, Phys. Rev. D **91**, 073010 (2015).
[34] I. Girardi, S. T. Petcov, and A. V. Titov, Predictions for the leptonic dirac *CP* violation phase: A systematic phenomenological analysis, Eur. Phys. J. C **75**, 345 (2015).
[35] I. Girardi, S. T. Petcov, A. J. Stuart, and A. V. Titov, Leptonic dirac *CP* violation predictions from residual discrete symmetries, Nucl. Phys. **B902**, 1 (2016).
[36] S. K. Kang, Minimal modification of tri-bimaximal neutrino mixing and leptonic *CP* violation, J. Korean Phys. Soc. **71**, 911 (2017).
[37] L. A. Delgadillo, L. L. Everett, R. Ramos, and A. J. Stuart, Predictions for the dirac *CP*-violating phase from sum rules, Phys. Rev. D **97**, 095001 (2018).
[38] S. T. Petcov and A. V. Titov, Assessing the viability of A_4, S_4 and A_5 flavour symmetries for description of neutrino mixing, Phys. Rev. D **97**, 115045 (2018).
[39] S. K. Kang, Y. Shimizu, K. Takagi, S. Takahashi, and M. Tanimoto, Revisiting A_4 model for leptons in light of NuFIT 3.2, Prog. Theor. Exp. Phys. **2018**, 083B01 (2018).
[40] S. P. Li, Yuan-Yuan-Li, X. S. Yan, and X. Zhang, Next-to-tribimaximal mixing against *CP* violation and baryon asymmetry signs, Phys. Rev. D **105**, 096008 (2022).
[41] W. Rodejohann and H. Zhang, Simple two parameter description of lepton mixing, Phys. Rev. D **86**, 093008 (2012).
[42] D. Marzocca, S. T. Petcov, A. Romanino, and M. C. Sevilla, Nonzero $|U_{e3}|$ from charged lepton corrections and the atmospheric neutrino mixing angle, J. High Energy Phys. 05 (2013) 073.

[43] Z. z. Xing and S. Zhou, A partial $\mu - \tau$ symmetry and its prediction for leptonic *CP* violation, Phys. Lett. B **737**, 196 (2014).

[44] Z. z. Xing and S. Zhou, Tri-bimaximal neutrino mixing and flavor-dependent resonant leptogenesis, Phys. Lett. B **653**, 278 (2007).

[45] X. G. He and A. Zee, Minimal modification to the tri-bimaximal neutrino mixing, Phys. Lett. B **645**, 427 (2007).

[46] C. S. Lam, Mass independent textures and symmetry, Phys. Rev. D **74**, 113004 (2006).

[47] C. H. Albright, A. Dueck, and W. Rodejohann, Possible alternatives to tri-bimaximal mixing, Eur. Phys. J. C **70**, 1099 (2010).

[48] X. G. He and A. Zee, Minimal modification to tri-bimaximal mixing, Phys. Rev. D **84**, 053004 (2011).

[49] M. C. Gonzalez-Garcia, M. Maltoni, and T. Schwetz, NuFIT: Three-flavour global analyses of neutrino oscillation experiments, Universe **7**, 459 (2021).

[50] L. L. Everett, R. Ramos, A. B. Rock, and A. J. Stuart, Predictions for the leptonic Dirac *CP*-violating phase, Int. J. Mod. Phys. A **36**, 2150228 (2021).

[51] NuFIT, www.nu-fit.org

[52] P. Huber, M. Lindner, and W. Winter, Simulation of long-baseline neutrino oscillation experiments with GLoBES (General Long Baseline Experiment Simulator), Comput. Phys. Commun. **167**, 195 (2005).

[53] P. Huber, J. Kopp, M. Lindner, M. Rolinec, and W. Winter, New features in the simulation of neutrino oscillation experiments with GLoBES 3.0: General long baseline experiment simulator, Comput. Phys. Commun. **177**, 432 (2007).

[54] B. Abi *et al.* (DUNE Collaboration), Deep underground neutrino experiment (DUNE), Far detector technical design report, Volume II: DUNE physics, arXiv:2002.03005.

[55] K. Abe *et al.* (Hyper-Kamiokande Collaboration), Physics potentials with the second Hyper-Kamiokande detector in Korea, Prog. Theor. Exp. Phys. **2018**, 063C01 (2018).

[56] M. Blennow, E. Fernandez-Martinez, T. Ota, and S. Rosauro (ESSnuSB Collaboration), Physics performance according to initial parameters, (2018), http://essnusb.eu/DocDB/public/ShowDocument?docid=205.

[57] L. Agostino, M. Buizza-Avanzini, M. Dracos, D. Duchesneau, M. Marafini, M. Mezzetto, L. Mosca, T. Patzak, A. Tonazzo, and N. Vassilopoulos (MEMPHYS Collaboration), Study of the performance of a large scale water-Cherenkov detector (MEMPHYS), J. Cosmol. Astropart. Phys. 01 (2013) 024.

[58] M. Blennow, M. Ghosh, T. Ohlsson, and A. Titov, Probing lepton flavor models at future neutrino experiments, Phys. Rev. D **102**, 115004 (2020).

[59] S. K. Agarwalla, S. S. Chatterjee, S. T. Petcov, and A. V. Titov, Addressing neutrino mixing models with DUNE and T2HK, Eur. Phys. J. C **78**, 286 (2018).

[60] M. Blennow, M. Ghosh, T. Ohlsson, and A. Titov, Testing lepton flavor models at ESSnuSB, J. High Energy Phys. 07 (2020) 014.

[61] I. de Medeiros Varzielas, S. F. King, and Y. L. Zhou, Multiple modular symmetries as the origin of flavor, Phys. Rev. D **101**, 055033 (2020).

[62] S. F. King and Y. L. Zhou, Trimaximal TM_1 mixing with two modular S_4 groups, Phys. Rev. D **101**, 015001 (2020).

[63] P. P. Novichkov, S. T. Petcov, and M. Tanimoto, Trimaximal neutrino mixing from modular A4 invariance with residual symmetries, Phys. Lett. B **793**, 247 (2019).

[64] F. Feruglio, Are neutrino masses modular forms?, arXiv:1706.08749.

[65] R. de Adelhart Toorop, F. Feruglio, and C. Hagedorn, Finite modular groups and lepton mixing, Nucl. Phys. **B858**, 437 (2012).

[66] P. P. Novichkov, J. T. Penedo, S. T. Petcov, and A. V. Titov, Generalised *CP* symmetry in modular-invariant models of flavour, J. High Energy Phys. 07 (2019) 165.

[67] T. Kobayashi, H. Ohki, H. Okada, Y. Shimizu, and M. Tanimoto, An introduction to non-abelian discrete symmetries for particle physicists, Lect. Notes Phys. **995**, 1 (2022).

[68] E. Ma and G. Rajasekaran, Softly broken A(4) symmetry for nearly degenerate neutrino masses, Phys. Rev. D **64**, 113012 (2001).

[69] K. S. Babu, E. Ma, and J. W. F. Valle, Underlying A(4) symmetry for the neutrino mass matrix and the quark mixing matrix, Phys. Lett. B **552**, 207 (2003).

[70] T. Kobayashi, K. Tanaka, and T. H. Tatsuishi, Neutrino mixing from finite modular groups, Phys. Rev. D **98**, 016004 (2018).

[71] J. C. Criado and F. Feruglio, Modular invariance faces precision neutrino data, SciPost Phys. **5**, 042 (2018).

[72] T. Kobayashi, N. Omoto, Y. Shimizu, K. Takagi, M. Tanimoto, and T. H. Tatsuishi, Modular A_4 invariance and neutrino mixing, J. High Energy Phys. 11 (2018) 196.

[73] H. Okada and M. Tanimoto, *CP* violation of quarks in A_4 modular invariance, Phys. Lett. B **791**, 54 (2019).

[74] T. Kobayashi, Y. Shimizu, K. Takagi, M. Tanimoto, T. H. Tatsuishi, and H. Uchida, Finite modular subgroups for fermion mass matrices and baryon/lepton number violation, Phys. Lett. B **794**, 114 (2019).

[75] H. Okada and M. Tanimoto, Towards unification of quark and lepton flavors in A_4 modular invariance, Eur. Phys. J. C **81**, 52 (2021).

[76] G. J. Ding, S. F. King, and X. G. Liu, Modular A_4 symmetry models of neutrinos and charged leptons, J. High Energy Phys. 09 (2019) 074.

[77] T. Kobayashi, Y. Shimizu, K. Takagi, M. Tanimoto, and T. H. Tatsuishi, A_4 lepton flavor model and modulus stabilization from S_4 modular symmetry, Phys. Rev. D **100**, 115045 (2019); Erratum, Phys. Rev. D **101**, 039904 (2020).

[78] T. Asaka, Y. Heo, T. H. Tatsuishi, and T. Yoshida, Modular A_4 invariance and leptogenesis, J. High Energy Phys. 01 (2020) 144.

[79] G. J. Ding, S. F. King, X. G. Liu, and J. N. Lu, Modular S_4 and A_4 symmetries and their fixed points: New predictive examples of lepton mixing, J. High Energy Phys. 12 (2019) 030.

[80] D. Zhang, A modular A_4 symmetry realization of two-zero textures of the Majorana neutrino mass matrix, Nucl. Phys. **B952**, 114935 (2020).

[81] H. Okada and M. Tanimoto, Modular invariant flavor model of A_4 and hierarchical structures at nearby fixed points, Phys. Rev. D **103**, 015005 (2021).

[82] P. T. P. Hutauruk, D. W. Kang, J. Kim, and H. Okada, Muon $g-2$ and neutrino mass explanations in a modular A_4 symmetry, arXiv:2012.11156.

[83] I. de Medeiros Varzielas and J. Lourenço, Two A4 modular symmetries for Tri-Maximal 2 mixing, Nucl. Phys. **B979**, 115793 (2022).
[84] G. Charalampous, S. F. King, G. K. Leontaris, and Y. L. Zhou, Flipped SU(5) with modular A4 symmetry, Phys. Rev. D **104**, 115015 (2021).
[85] A. Dasgupta, T. Nomura, H. Okada, O. Popov, and M. Tanimoto, Dirac radiative neutrino mass with modular symmetry and leptogenesis, arXiv:2111.06898.
[86] T. Nomura, H. Okada, and Y. h. Qi, Zee model in a modular A_4 symmetry, arXiv:2111.10944.
[87] T. Kobayashi, H. Otsuka, M. Tanimoto, and K. Yamamoto, Modular symmetry in the SMEFT, Phys. Rev. D **105**, 055022 (2022).
[88] H. Okada and M. Tanimoto, Spontaneous CP violation by modulus τ in A_4 model of lepton flavors, J. High Energy Phys. 03 (2021) 010.
[89] X. G. Liu and G. J. Ding, Modular flavor symmetry and vector-valued modular forms, J. High Energy Phys. 03 (2022) 123.
[90] T. Nomura and H. Okada, A radiative seesaw model in a supersymmetric modular A_4 group, arXiv:2201.10244.
[91] H. Otsuka and H. Okada, Radiative neutrino masses from modular A_4 symmetry and supersymmetry breaking, arXiv:2202.10089.
[92] N. Aghanim *et al.* (Planck Collaboration), Planck 2018 results. VI. Cosmological parameters, Astron. Astrophys. **641**, A6 (2020); Erratum, Astron. Astrophys. **652**, C4 (2021).